Accepted Manuscript

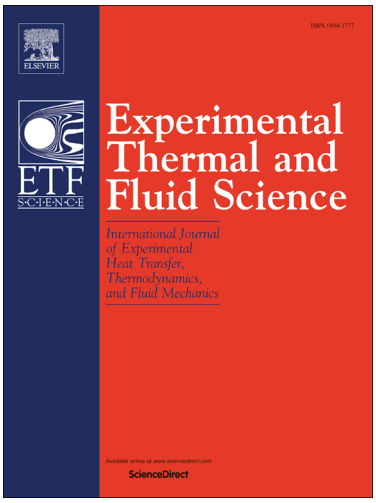

Optimization of a solar air heater with phase change materials: Experimental and numerical study

Ramin Moradi, Ali Kianifar, Somchai Wongwises

PII: S0894-1777(17)30207-8
DOI: http://dx.doi.org/10.1016/j.expthermflusci.2017.07.011
Reference: ETF 9153

To appear in: *Experimental Thermal and Fluid Science*

Received Date: 15 January 2017
Revised Date: 12 July 2017
Accepted Date: 18 July 2017

Please cite this article as: R. Moradi, A. Kianifar, S. Wongwises, Optimization of a solar air heater with phase change materials: Experimental and numerical study, *Experimental Thermal and Fluid Science* (2017), doi: http://dx.doi.org/10.1016/j.expthermflusci.2017.07.011

Optimization of a solar air heater with phase change materials: Experimental and numerical study

Ramin Moradi[a], Ali Kianifar[a,*], Somchai Wongwises[b,c*]

[a] Department of Mechanical Engineering, Engineering Faculty, Ferdowsi University of Mashhad, Iran

[b]Fluid Mechanics, Thermal Engineering and Multiphase Flow Research Lab. (FUTURE),
Department of Mechanical Engineering, Faculty of Engineering,
King Mongkut's University of Technology Thonburi,
Bangmod, Bangkok 10140, Thailand

[c] The Academy of Sciences, Royal Society of Thailand,
Sanam Suea Pa, Dusit, Bangkok 10300

*Corresponding authors: a-kiani@um.ac.ir (A. Kianifar)

somchai.won@kmutt.ac.th (S.Wongwises)

Abstract

In this paper, a solar air heater (SAH) with phase change material (PCM)-based energy storage is investigated. Paraffin was placed underneath the absorber plate as the PCM. A transient two-dimensional laminar model was used in the Ansys Fluent 17 software to study the effects of different parameters on the performance of the SAH, such as the air mass flow rate, the amount of paraffin, and the thermal conductivity of the paraffin. The performance of the SAH was optimized by considering two objectives simultaneously: thermal energy efficiency and maximum nocturnal temperature difference between the inlet and the outlet of the SAH. To validate the numerical model, a SAH with a 2-cm paraffin layer and the same dimensions as the numerical model was built and tested. The results of the simulation showed good agreement with the experimental results.

Keywords : Solar Energy; Solar Air Heater; Phase Change Material (PCM); Energy Storage

1. Introduction

Although solar energy is the most abundant and accessible form of renewable energy in nature, its time-dependent nature is a major disadvantage [1], and storing the solar energy as a reliable source is

still a serious problem. Thermal energy storage systems are useful solutions for this problem and facilitate the deployment of solar energy.

The main solutions for storing thermal energy include using the sensible heat of materials (solid or liquid) and the latent heat of phase change materials (PCMs). PCMs store and release thermal energy through the process of melting and freezing. Latent heat-based energy storage has advantages over sensible heat-based energy storage, such as the ability to control the maximum temperature, more energy value by mass and/or volume, and easy installation in domestic systems. For example, some thermal systems need to operate in roughly constant temperatures to achieve higher efficiency [2]. A wide variety of materials can be used as PCMs, as comprehensively reviewed by Atul Sharma et al. [3].

PCMs are applicable to different engineering applications, such as energy storage at buildings, glazing and shading in buildings, greenhouse heating, electronic products, drying applications, restoring heat loss, chilling and cold storage, solar air heaters, and solar cookers [4-17]. Regarding the space requirements for the energy storage, a comparison between water and a PCM such as sodium sulfate decahydrate (Glauber's salt) shows that water requires almost five times the amount of space as salt. This space savings leads to reduced construction and insulation costs in buildings, and it is considered the most significant advantage of PCMs in building applications [18]. On the other hand, Panna Lal Singh et al. [19] compared rock bed and paraffin in a SAH and concluded that sensible heat storage had slightly better heat-retrieval efficiency. Moreover, the efficiency of their system's solar energy collection was between 36% and 51%, and the system could restore around 76% of the collected solar energy during the discharge period. Different factors must be considered when choosing a suitable PCM for a system, such as a suitable melting point, a high heat transfer coefficient, high fusion heat, high density, low volume change by pressure, low vapor pressure, high chemical stability, non-toxic properties, non-fire properties, low price, abundance, and availability [3]. Therefore, the PCM is chosen based on the working conditions. The main criterion in choosing the PCM is the melting temperature point of the material; for example, most research uses paraffin as the PCM in domestic systems [20].

Hammou and Lacroix [21] studied a mixed solar–electrical heating system utilizing PCM for energy storage. The system reduced electricity consumption by up to 32%, and 90% of the electricity was consumed during off-peak hours. Mettawee and Assassa [22] designed a solar water heater with paraffin as the PCM. The experimental results showed that the average heat transfer coefficient increased during the charging period (when the paraffin turned to liquid), in keeping with the increased thickness of the melted layers of paraffin as the natural convection strengthened. Alkilani et

al. [23] predicted the freezing time of paraffin during the discharging period of a single-glazed SAH. They used cylinders filled with paraffin as an absorber-container and mixed paraffin with aluminum powder at a mass fraction of 0.5% to improve its heat-transfer coefficient. The study indicated that freezing time had an inverse relationship with the mass flow rate of air. At best, the freezing time was approximately 8 hr at a mass flow rate of 0.05 kg/s. Benli and Durmus [24] researched the performance of a SAH designed for greenhouse space heating, and they picked $CaCl_2.6H_2O$ as the PCM with a melting temperature of 29 °C. The system created a temperature difference to 9 °C between the inside and the outside of the greenhouse, and it could supply around 20% of the greenhouse's daily energy demand for 3–4 hr. Salwa Bouadila et al. [25] designed a SAH with packed-bed latent heat-based energy storage. The main goal of their design was nocturnal use of solar energy. The overall daily energy efficiency of their system was between 32% and 45%, and the daily exergy efficiency was between 13% and 25%.

In most cases, such as with alloys and impure materials, the phase change occurs over a range of temperatures, and the material appears between the solid and the liquid phase during the *plastic phase* [26]. Studies have shown that the low heat-transfer coefficient of PCMs usually poses a common thermal problem [27]. Various studies have put forward a set of solutions to tackle this problem, such as encapsulation of the PCM, as comprehensively reviewed by Jessica Giro Paloma et al. [28], and the use of carbon fibers and graphite foams in the PCM, as reviewed by Shalaby et al. [29].

Overall, the pros of numerical studies lie in the ability to analyze non-linear phenomena and complex geometries, which are difficult to solve analytically. Moreover, it is possible to assess the system at any moment, which is inaccessible in experiments. However, its major cons include the convergence of answers, the restrictions on the boundary conditions, and the computation costs [30]. TRNSYS and EES are the most recommended software packages with which to simulate SAHs. A comprehensive review of studies utilizing common software is available in the literature [31].

Another approach to find the optimized performance of systems is inverse modeling. In this case, values of some effective input variables are estimated to satisfy prescribed performance of the system. Researchers used different optimization algorithms to solve inverse problems, especially nature-inspired algorithms, which have been stated as reliable methods. Ranjan Das et al. [32] used Artificial Bee Colony (ABC) algorithm to achieve the preferred heat loss factor of a double-glazed solar collector in domestic water heating system. They optimized five parameters simultaneously for satisfying a given distribution of heat loss factor using the ABC algorithm while the ambient condition was assumed constant. Using this method, the size of the collector was reduced by 6 to 32%, and the absorber plate emissivity was introduced as a significant parameter to control the heat

loss factor of the collector. Srikumar Panda et al. [33] utilized finite difference method (FDM) in conjunction with binary-coded genetic algorithm (GA) to optimize thermo-physical parameters in a flat-plate solar collector. Parameters were optimized including thermal conductivity of the absorber plate, overall heat loss coefficient and incident solar heat flux to achieve a prescribed temperature field. Using this optimization method, they proposed suitable materials for the absorber plate and different locations satisfying a given temperature field in the collector. Arka Bhowmik et al. [34] compared three optimization methods to estimate unknown parameters satisfying a given temperature field in a flat-plate solar collector. The methods were golden section search method (GSSM), simplex search method (SSM) and differential evolution (DE), while analytical forward method was used by considering Fourier and non-Fourier heat conduction to calculate the temperature field. They reported that estimating unknown parameters, which were Fourier number (Fo), Vernotte number (Ve), and non-dimensional solar heat flux (S^*), requires accurate measurement of the temperature field; otherwise, unrealistic estimation can be observed. In addition, they suggested that direct search methods (GSSM and SSM) were more efficient compared to evolutionary method (DE) for estimating the previously mentioned parameters.

A majority of the computational fluid dynamics (CFD) studies on SAHs used ANSYS Fluent software, and researchers used the different models offered by ANSYS Fluent. The results of 2-D numerical models are generally close to those of 3-D numerical models but with considerably lower computational costs [2]. A research that is similar to our study in case of size of the SAH, Edward Summers et al. [35] conducted a numerical study (with a two-dimensional finite element model using ADINA software) on a double-glazed SAH with commercial paraffin as the PCM. They concluded that the nocturnal outlet temperature had maximum constancy at an air mass flow rate of 47 kg/s, and the maximum outlet temperature was close to the melting temperature of the paraffin. In addition, the nocturnal temperature had an inverse relationship with the energy efficiency. Despite the merits of the CFD analysis of SAHs, few CFD studies have been conducted in comparison with studies with an experimental approach [30].

This paper studies a SAH with phase change-based energy storage to optimize its performance under charging and heat-retrieval modes. The effects of three variables on the performance of the SAH were evaluated using numerical simulation. To do so, the near-optimum value of one variable was found by altering its value while the other two were kept constant. Next, the second variable was altered while the third was considered constant, and the first was held at the near-optimum value found in the previous step. This was also done for the third variable. A transient 2-D laminar model available in the CFD code of Fluent 17 was used and validated by experimental tests. The goal of the optimized

system is to achieve acceptable overall energy efficiency and nocturnal outlet temperatures at the same time. Furthermore, the amount of the PCM under the absorbent and the size of the SAH were optimized to reduce construction costs. In addition, inexpensive packing for the PCM was devised in the experiments, which was effective in the heat transfer to the PCM as well.

2. Experimental setup

In this study, a double-glazed SAH was built and tested in Bojnourd, located in northeast Iran, with latitude, longitude, and altitude of 37.3°, 57.2°, and 1150 m, respectively. Figure 1 shows the SAH along with a schematic of its configuration and its dimensions. Air flows between the absorber plate and the first glazing and then exits from the other side of the collector as a single-pass flow.

Paraffin was placed under the absorber plate as the PCM. The outlet temperature was measured and recorded over 24 hr at 15-min intervals using a T-type thermocouple, and the data for ambient temperature and daily variation in solar radiation were obtained from a meteorological center located 4 km from the experiment site. Solar radiation was measured using a commercial pyranometer with an accuracy of 20 W/m^2. This instrument measures the sum of the beam solar radiation and the sky diffuse radiation on a horizontal surface. A pitot tube connected to a digital manometer was used to measure the mass flow rate of the air.

A galvanized sheet was used to fabricate the body of the SAH, for which glass wool with a thickness of 5 cm was used as the insulator. The absorber plate was made out of a galvanized steel sheet with a thickness of 1.25 mm and painted matte black. Increasing the roughness of the absorbent is a common way to improve the convection heat transfer coefficient [36]. Therefore, the absorber plate was sprinkled with crushed coal— a non-selective coating—to decrease the smoothness of the surface. Selective coatings on the absorber plate significantly enhance the collector's performance in absorbing the maximum solar radiation but have high cost, low productivity, and complex processes [37]. The collector was installed at an angle of about 30° to the horizontal and oriented to the south. A fan was attached to the outlet and equipped with a voltage regulator, so that the airflow rate could be altered.

In this study, aluminum powder with 0.5% of paraffin weight was added to pure paraffin to improve its heat transfer coefficient (about 0.2 W/m.K) with respect to previous studies [23]. Furthermore, paraffin wax was packed into thin plastic packs, and two sheets of aluminum were placed inside of each pack to improve the heat transfer to the paraffin. Table 1 presents the thermophysical properties of the paraffin. The numerical study and other calculations used the same values.

A stack of packages was placed under the absorber plate regularly to form a layer of paraffin, and approximately 11 kg of wax was used to shape a 2-cm paraffin layer. The density and the melting point of the paraffin were measured in our laboratory, while other properties were extracted from Agyenim et al. [38].

3. Numerical modeling

3-1. Grid and model

In this study, the Fluent 17 software was used to carry out a numerical simulation. A non-uniform triangular grid was used to build up the computational domain in the Gambit 2.3 software, with a total number of 90,727 cells (for 2-cm thickness of paraffin). A transient 2-D laminar model was chosen to simulate the SAH. Because of the availability of hourly ambient temperature and solar radiation on July 5, 2016, they were assumed constant for each hour in the numerical simulation. Therefore, constant irradiation was set perpendicular to the absorbent on the upper glazing and equal to the hourly solar irradiation, and constant temperature was assumed for the inlet air for each hour. A discrete ordinates (DO) model was selected to help consider the effects of radiative heat transfer.

In addition, the SAH body was assumed to be fully insulated; thus, the boundary condition of the body was zero heat flux. Nevertheless, the simulation considered heat loss from the glazing. In addition, the outlet boundary condition of the SAH was zero gauge pressure, and the density and the specific heat of air were assumed to be constant ($c_p = 1.005\,kJ/kg.m^3$, $\rho = 1.1\ kg/m^3$). In Fluent, mass flow inlet and pressure outlet were selected for the boundary conditions of inlet and outlet of the SAH, respectively, as shown in figure 2.

Table 2 represents the material properties based on common material tables, and the numerical simulation used the same values. The properties of paraffin were assumed to be equal to the experimental values mentioned in the previous section.

3-2. Solidification and melting formulation

The phase change was analyzed by using the enthalpy method in Fluent software [39]. This software calculates the melting fraction, rather than using the split-second calculation of the melted surface. The melting fraction for every cell in each phase is calculated by means of an iterative solution of the energy equation (written based on the enthalpy). Voller and Prakash present details on the enthalpy-porosity method [40]. The melting fraction is a number between zero and one allocated to each cell. Zero indicates the solid phase, one signifies the liquid phase, and a number between zero and one signifies the plastic phase.

The energy equation based on enthalpy is as follows:

$$\partial_t(\rho H) + \nabla(\rho \bar{v} H) = \nabla(k \nabla T) + S, \quad (1)$$

where ρ is the density, $\bar{v}$ is the average fluid velocity, k is the heat transfer coefficient, S is the source term (for details of the source term, refer to [2] or [39]), and H is the enthalpy. H is defined below:

$$H = h + \Delta H. \quad (2)$$

H represents the total enthalpy of the material and is calculated using the following equation:

$$h = h_{ref} + \int_{T_{ref}}^{T} c_p \Delta T, \quad (3)$$

where h_{ref} is the enthalpy at the reference temperature of T_{ref} and c_p is the specific heat of the material. Note that ΔH is the latent heat of the material based on a fraction of the material's heat of fusion, which is defined as:

$$\Delta H = \gamma \, . \, L, \quad (4)$$

where L is the latent heat capacity and γ is the liquid fraction that appears during the phase change between the solid and the liquid state when the temperature lies between T_l and T_s:

$$\gamma = \begin{cases} 0 & if \quad T < T_s \\ 1 & if \quad T > T_l \\ (T - T_s)/(T_l - T_s) & if \quad T_l > T > T_s \end{cases} \quad (5)$$

After determining its value, it is possible to calculate the phase and the temperature of the material.

4. Analytical energy equations

The basis of the theoretical model is the energy balance, in terms of the first law of thermodynamics:

$$Q_A = Q_u + Q_{st} + Q_{los} \quad (6)$$

Note that Q_A, Q_u, Q_{st}, and Q_{los} are the absorbed heat, useful heat, stored heat, and lost heat, respectively. The useful energy is calculated as follows:

$$Q_u = \dot{m} c_p (T_o - T_i). \quad (7)$$

The total energy efficiency is calculated below:

$$Eff_{tot} = \frac{Q_u}{A_c I_T}. \quad (8)$$

Equation (8) shows the ratio of useful energy collected by the collector to the solar energy radiated onto the external surface of the collector. In this equation, Q_u is the overall useful energy during a 24-hr period.

The discharging thermal efficiency can be calculated from the ratio of the overall useful energy gained from the collector during the discharging period to the overall solar energy radiated onto the collector's surface:

$$Eff_{\text{dis}} = \left(\int_{dis} Q_{dis}\right) \Big/ \left(\int_{ch} A_c I_T\right). \quad (9)$$

Also, energy storage efficiency is the ratio of the energy gained during the discharging period to the total energy storage capacity of the paraffin and is calculated as follows:

$$Eff_{st} = \frac{Q_{dis}}{ml_f}. \quad (10)$$

5. Validation of the results

To validate the numerical results, they were compared with the experimental results at a flow rate of 46 kg/hr considering 2 cm of paraffin under the absorber plate. A SAH was constructed with the same dimensions as the numerical model, and it was tested in various weather conditions. The experiment was run at a steady state during three successive days to eliminate the effects of the initial flow. The charging period was between 5:30 a.m. and 6:30 p.m., and solar radiation was considered zero after 6:30 p.m. in the numerical study.

Figure 3a shows the outlet temperatures of the SAH (simulated and experimental) and the ambient temperature on July 5, 2016. There is rather good agreement between the numerical and experimental results. Furthermore, Figure 3b shows that the difference between the results grew during sunny hours. The reason for this discrepancy was the difference between the experimental conditions and the numerical assumptions, including the air gap between the absorber plate and the paraffin in the experiment; heat loss from the body (not glazing) of the SAH, which was assumed to be zero; and measurement errors.

6. Uncertainty analysis

Uncertainty analysis can effectively show the accuracy of experimental results. Two types of standard uncertainty are investigated by Jianfeng Yu et al. [41]: the standard uncertainty of measurement tools and

the standard uncertainty of testing data. The standard deviation of each uncertainty component is calculated using equation (11):

$$\sigma_s = \frac{\delta}{\sqrt{3}}, \quad (11)$$

where δ is the accuracy of the measurement tools (for example, 1 ℃ for the thermocouple and 1 pa for the digital manometer in our experiments).

Moreover, repetition of the experiment revealed that another source of uncertainty in the results originated from any valid method for testing data:

$$u_i = \frac{s}{\sqrt{n}}, \quad (12)$$

where u_i is the standard uncertainty of x_i, n is the number of the repetitions of the measurement, and s is the total standard deviation of the mean:

$$s = \sqrt{\frac{\Sigma(x_i - \bar{x})^2}{n-1}}, \quad (13)$$

where x_i indicates a value as the individual measurement and $\bar{x}$ is the mean of the measurements.

Eventually, the total uncertainty of the measurement is calculated as follows:

$$u_{tot} = \sqrt{{\sigma_s}^2 + {u_i}^2} \quad (14)$$

Results from three consecutive days were used to calculate the standard uncertainty of the outlet temperature. Therefore, variable n in Eqs. 12 and 13 is equal to 3, and δ is equal to 1 $^{\circ}$C. Table 3 summarizes the values for the standard uncertainty of hourly outlet temperature on July 5, 2016. Figure 4 shows an estimation of the uncertainty analysis of the outlet temperature on July 5, 2016.

7 Results and discussion

In this section, the effects of some variables on the performance of the SAH are examined using the CFD approach. The input variables in all of the simulations were taken from the weather conditions on July 5, 2016.

7.1 Air flow rate

Figure 5 shows a diagram of the average outlet temperature in terms of the passing airflow rate through the SAH (zero indicates 6:00 a.m. on the graphs). The thickness of the paraffin under the

absorber plate was 2 cm. The nocturnal temperature difference indicates the system's capability to store solar energy. Regarding the same amount of energy delivered to the air stream, a higher mass flow indicates a lower temperature difference between the inlet and the outlet.

The overall thermal power was calculated by adding up the hourly thermal power during a 24-hr period, and the stored energy was calculated by summing the hourly thermal power during the discharging period (from 6:30 p.m. to 5:30 a.m. the next morning). The average nocturnal temperature difference was the average temperature difference between the outlet and inlet of the SAH during the discharging period.

As can be seen in Figure 6, the average nocturnal temperature difference decreased in inverse proportion to increases in the flow rate. In addition, the total thermal energy rises when the flow rate goes up to 85 kg/hr, and it does not change considerably for higher values.

Figure 7 shows that the total thermal efficiency of the SAH varied between 35% and 45%, and about 13% to 15% of the thermal efficiency was obtained during the discharging period. Discharging efficiency had a nearly constant value and was not dependent on the airflow rate. Moreover, between 75% and 90% of the paraffin's total heat of fusion was obtained during the night. In addition, the total energy efficiency and energy storage efficiency had optimum values at an airflow rate of about 85 kg/hr.

Figure 8 shows the liquid fraction contour of the paraffin at 5:30 p.m. given three airflow rates. The X indicates the entry length of the collector at which no significant phase change occurred in the PCM. Length X was taken from the bottom of the tank and is called *dead length* in this paper. The melting fraction of paraffin has a value between zero and 0.75 at this length. The dead length increases as the airflow rate increases, which leads to decreased storage efficiency at a flow rate of 125 kg/hr, as illustrated in Figure 7.

Figure 9 shows the dimensionless dead length $l = X/L$ (where L is the length of the absorber plate) based on the Reynolds number (based on hydraulic diameter of the air duct) of the airflow through the SAH. The dimensionless dead length increases with an approximately constant slope as the Reynolds number increases. Implementing a PCM at this inlet distance not only has no consequential effect for storing thermal energy but also imposes extra costs.

The optimized airflow rate for both energy efficiency and the nocturnal temperature difference is nearly 65 kg/hr. the SAH must operate at a lower flow rate to achieve a greater nocturnal temperature difference, leading to the thermal inefficiency of the SAH. The following results were produced at an airflow rate of 65 kg/hr.

7.2 Thermal conductivity of PCM

The low thermal conductivity of paraffin can cause considerable thermal resistance in front of the heat transfer between the paraffin and the absorber plate. As a result, the internal layers of paraffin cannot be completely melted. To overcome this problem, researchers have used various methods to improve the thermal conductivity of paraffin, as mentioned in the Introduction.

Figure 10 shows the energy efficiencies defined in this paper, the average nocturnal temperature difference in the paraffin's thermal conductivity at an airflow rate of 65 kg/hr, and the efficiencies with 4 cm of paraffin under the absorber plate. As clearly seen, the total energy efficiency does not change considerably when the paraffin's thermal conductivity changes. In addition, the near-optimum performance of the SAH can be found when the thermal conductivity exceeds 1 W/m.K.

7.3 The thickness of PCM

Accurate determination of the optimum amount of PCM plays a significant role in the energy efficiency and costs of a SAH. Figure 11 shows the useful thermal energy calculated from equation (7) by the thickness of the paraffin layer at an air mass flow rate of 65 kg/hr. Both the total and the charging thermal energy graphs fall as the paraffin thickness increases. During the charging period and with more paraffin under the absorber plate, solar energy is consumed to heat up a larger amount of paraffin, which lowers the absorbent temperature. The charging thermal energy is reduced as a result of this heat sink.

On the other hand, solar energy heats up the paraffin deep inside the paraffin layers during the charging period, but this energy cannot be completely restored during the discharging period due to the lower temperature differences between the absorber plate and the paraffin at night compared with the daytime, which reduces the total thermal energy. This is also true for discharging thermal energy for any paraffin thickness greater than 4 cm as shown in figure 12.

Figure 13 shows the energy efficiencies and the average nocturnal temperature differences by thickness of the paraffin layer. As the diagram indicates, an increase in the thickness of the paraffin layer leads to a reduction in the total energy efficiency of the SAH. This intensifies the energy storage efficiency, as the thermal storage capacity increases while the useful thermal energy at the discharging period declines. This can be explained by the thermal energy graphs in Figure 11. Furthermore, the discharging efficiency has a near-optimum value when the paraffin thickness is 4 cm. Considering this and the average nocturnal temperature difference curve, 4 cm of paraffin under the absorbent results in better performance of the SAH. Table 4 presents a summary of the optimization results elaborated in section 7.

8 Conclusion

A SAH with integrated PCM storage was designed for this paper. A transient two-dimensional laminar model was used in the Fluent 17 software to optimize the performance of the SAH. The numerical results were validated by experiments, and the results were found to be in good agreement. The SAH was investigated considering the two simultaneous objectives of the design stage: appropriate energy efficiency and maximum nocturnal temperature difference between the inlet and the outlet of the SAH. With respect to the results, the following conclusions were obtained:

- About one-third of the total thermal energy was obtained during the discharging period when using the PCM under the absorber plate. This could increase the total thermal efficiency of the system considerably.
- The SAH, at its best, was able to keep the average nocturnal temperature difference at 4.5 $^{\circ}$C using 23.5 kg of paraffin (a layer with 4 cm thickness under the absorber plate), and the total energy efficiency was about 37% at an airflow rate of 65 kg/hr.
- Increasing the thermal conductivity of the paraffin results in greater nocturnal temperature differences between the inlet and the outlet of the SAH. This is more important when its value is under 1 W/m.K.
- The paraffin did not melt in regions near the inlet of the SAH. In this paper, this region is introduced as a dimensionless length, and its value climbed with a roughly constant slope, keeping with the rise in the Reynolds number of the passing air. The dead length should be taken into consideration during the design stage to diminish the allocated space for the PCM.
- The determination of an adequate amount of paraffin has a significant impact on the economic aspects of the SAH, its weight, and the space occupied by the PCM. The results showed that implementing 4 cm of paraffin resulted in near-optimum performance for the SAH.

Acknowledgement

The authors appreciate the Department of Mechanical Engineering, Ferdowsi University of Mashhad, Iran for the financial support provided for this research. The third author also acknowledges the support provided by the "Research Chair Grant" National Science and Technology Development Agency (NSTDA), the Thailand Research Fund (TRF), the National Research University (NRU) Project and King Mongkut's University of Technology Thonburi through the "KMUTT 55th Anniversary Commemorative Fund".

Nomenclature			
H	Enthalpy (J/kg)	Greek Symbols	
k	Thermal conductivity (W/m.K)	ρ	Density (kg/m^3)
T	Temperature (K)	Δ	Difference operator
C_p	Specific heat (J/kg.K)	$\bar{v}$	Average fluid velocity (m/s)
Q_A	Absorbed heat (J)	γ	Melting fraction
Q_u	Useful heat (J)	δ	Accuracy of the measurement tool
Q_{st}	Stored heat (J)		
Q_{los}	Loses heat (J)	Subscripts and abbreviations	
$\dot{m}$	Air mass flow rate (kg/S)	ref	Reference
T_{out}	Air outlet temperature (K)	s	Solid phase
T_{in}	Air inlet temperature (K)	l	Liquid phase
m	PCM mass (kg)	Amb	Ambient
A_c	Absorber cross section area (m^2)	PCM	Phase Change Material
I_T	Solar intensity (kJ/m^2)	Eff	Efficiency
$\boldsymbol{u}$	Uncertainty	St	Stored
$\mathbf{l_f}$	Latent heat of fusion (kJ/kg)	Tot	Total
ΔT	Average nocturnal temperature difference	Ch	Charge
Re	Reynolds number based on hydraulic diameter	Dis	Discharge
$\boldsymbol{T_l}$	Liquidus Temperature (K)	SAH	Solar Air Heater
$\boldsymbol{T_s}$	Solidus Temperature (K)	CFD	Computational Fluid Dynamics
σ_s	Total standard deviation	avg	Average

References

[1] Duffie JA and Beckman WA, "Solar Engineering of Thermal Processes, Third edition," *John Wiley & Sons,* 2006.

[2] Abduljalil A.Al-abidi, Sohif Bin Mat, K.Sopian, M.Y.Sulaiman, and Abdulrahman Th.Mohammed, "CFD applications for latent heat thermal energy storage: a review," *Renewable and Sustainable Energy Reviews,* vol. 20, pp. 353-63, 2013.

[3] Atul Sharma, V.V.Tyagi, C.R.Chen, and D.Buddhi, "Review on thermal energy storage with phase change materials and applications," *Renewable and Sustainable Energy Reviews,* vol. 13, pp. 318-45, 2009.

[4] Azzouz K, Leducq D, and Gobin D, "Performance enhancement of a household refrigerator by addition of latent heat storage," *International Journal of Refrigeration,* vol. 31, pp. 892-901, 2008.

[5] Azzouz K, Leducq D, and Gobin D, "Enhancing the performance of household refrigerators with latent heat storage: an experimental investigation," *International Journal of Refrigeration,* vol. 32, pp. 1634-44, 2009.

[6] C- akmak G and Yıldız C, "The drying kinetics of seeded grape in solar dryer with PCM-based solar integrated collector," *Food and Bio products Processing,* vol. 89, pp. 103-8, 2011.

[7] Khalid A. Joudi and Ammar A. Farhan, "Greenhouse heating by solar air heaters on the roof," *Renewable Energy,* vol. 72, pp. 406-414, 2014.

[8] Mahmud A, K S, A. AM, and Sohif M, "Using a paraffin wax-aluminum compound as a thermal storage material in solar air heater," *Journal of Engineering and Applied Sciences,* vol. 4, pp. 74-7, 2009.

[9] Murat Kenisarin and Khamid Mahkamov, "Passive thermal control in residential buildings using phase change materials," *Renewable and Sustainable Energy Reviews,* vol. 55, pp. 371-98, 2016.

[10] Oro´ E, Miro´ L, Farid MM, and Cabeza LF, "Improving thermal performance of freezers using phase change materials," *International Journal of Refrigeration,* vol. 35, pp. 984-91, 2012.

[11] Pandiyarajan V, Chinna Pandian M, Malan E, Velraj R, and Seeniraj RV, "Experimental investigation on heat recovery from diesel engine exhaust using finned shell and tube heat exchanger and thermal storage system," *Applied Energy,* vol. 88, pp. 77-87, 2011.

[12] Sharma SD, Iwata T, Kitano H, and Sagara K, "Thermal performance of a solar cooker based on an evacuated tube solar collector with a PCM storage unit," *Solar Energy,* vol. 78, pp. 416-26, 2005.

[13] Shatikian V, Ziskind G, and Letan R, "Numerical investigation of a PCM-based heat sink with internal fins:constant heat flux," *Int J Heat and Mass Transfer,* vol. 51, pp. 1488-93, 2008.

[14] Tan H, Li C, and Li Y, "Simulation research on PCM freezing process to recover and store the cold energy of cryogenic gas," *International Journal of Thermal Sciences,* vol. 50, pp. 2220-7, 2011.

[15] Tiago Silva, Romeu Vicente, and Fernanda Rodrigues, "Literature review on the use of phase change materials in glazing and shading solutions," *Renewable and Sustainable Energy Reviews,* vol. 53, pp. 515-35, 2016.

[16] Wang Y-H and Yang Y-T, "Three dimensional transient cooling simulations of a portable electronic device using PCM(phase change materials) in multi-fin heat sink," *Energy,* vol. 36, pp. 5214-24, 2011.

[17] Yang Y-T and Wang Y-H, "Numerical simulation of three-dimensional transient cooling application on a portable electronic device using phase change material," *International Journal of Thermal Sciences,* vol. 51, pp. 155-62, 2012.

[18] Mahmud M. Alkilani, K. Sopian, M.A. Alghoul, M. Sohif, and M.H. Ruslan, "Review of solar air collectors with thermal storage units," *Renewable and Sustainable Energy Reviews,* vol. 15, pp. 1476-90, 2011.

[19] Panna Lal Singh, S.D. Deshpandey, and P. C. Jena, "Thermal performance of packed bed heat storage system for solar air heaters," *Energy for Sustainable Development,* vol. 29, pp. 112-17, 2015.

[20] Adeel Waqas and Zia Ud Din, "Phase change material (PCM) storage for free cooling of buildings – A review," *Renewable and Sustainable Energy Reviews,* vol. 18, pp. 607-25, 2013.

[21] Hammou ZA and Lacroix M, "A new PCM storage system for managing simultaneously solar and electric energy," *Energy and Buildings* vol. 38, pp. 258-65, 2006.

[22] Mettawee E-B and Assassa GMR, "Experimental study of a compact PCM solar collector," *Energy,* vol. 31, pp. 2958-68, 2006.

[23] Alkilani MM, Sopian K, Sohif M, and Alghol M, "Output air temperature prediction in a solar air heater integrated with phase change material European.," *J Sci Res,* vol. 27(3), pp. 334-41, 2009.

[24] Benli H and Durmus A, "Performance analysis of a latent heat storage system with phase change material for new designed solar collectors in greenhouse heating," *Solar Energy,* vol. 83, pp. 2109-19, 2009.

[25] Salwa Bouadila, Sami Kooli, Mariem Lazaar, Safa Skouri, and Abdelhamid Farhat, "Performance of a new solar air heater with packed-bed latent storage energy for nocturnal use," *Applied Energy,* vol. 110, pp. 267-75, 2013.

[26] Prashant Verma, varun, and S.K. Singal, "Review of mathematical modeling on latent heat thermal energy storage systems using phase-change material," *Renewable and Sustainable Energy Reviews,* vol. 12, pp. 999-1031, 2008.

[27] Adebiyi GA, "A second law study on packed bed energy storage systems utilizing phase change materials," *ASME Journal Solar Energy Engineering,* vol. 113, pp. 146-56, 1991.

[28] Jessica Giro Paloma, Monica Martinez, Luisa F. Cabeza, and A. Ines Fernandez, "Types, methods, techniques, and applications for micro encapsulated phase change materials (MPCM): A review," *Renewable and Sustainable Energy Reviews,* vol. 53, pp. 1059-75, 2016.

[29] S.M. Shalaby, M.A.Bek, and A.A.El-Sebaii, "Solar dryers with PCM as energy storage medium: A review," *Renewable and Sustainable Energy Reviews,* vol. 33, pp. 110-116, 2014.

[30] Anil Singh Yadav and J.L. Bhagoria, "Heat transfer and fluid flow analysis of solar air heater: A review of CFD approach," *Renewable and Sustainable Energy Reviews,* vol. 23, pp. 60-79, 2013.

[31] Abhishek Saxena, Varun, and A.A.El-Sebaii, "A thermodynamic review of solar air heaters," *Renewable and Sustainable Energy Reviews,* vol. 43, pp. 863-890, 2015.

[32] Ranjan Das, Bahriye Akay, Rohit K. Singla, and Kuljeet Singh, "Application of artificial bee colony algorithm for inverse modelling of a solar collector," *Inverse Problems in Science and Engineering,* vol. 25, pp. 887-908, 2016.

[33] Srikumar Panda, Rohit K. Singla, Ranjan Das, and Subash C. Martha, "Identification of design parameters in a solar collector using inverse heat transfer analysis," *Energy Conversion and Management,* vol. 88, pp. 27-39, 2014.

[34] Arka Bhowmik, Rohit K. Singla, Ranjan Das, A. Mallick, and R. Repaka, "Inverse modeling of a solar collector involving Fourier and non-Fourier heat conduction," *Applied Mathematical Modelling,* vol. 38, pp. 5126-48, 2014.

[35] Edward K. Summers, Mohammed A. Antar, and John H. Lienhard V, "Design and optimization of an air heating solar collector with integrated phase change material energy storage for use in humidification–dehumidification desalination," *Solar Energy,* vol. 86, pp. 3417-29, 2012.

[36] Hakan G. Oztop, Fatih Bayrak, and Arif Hepbasli, "Energetic and exergetic aspects of solar air heating (solar collector) systems," *Renewable and Sustainable Energy Reviews,* vol. 21, pp. 59-83, 2013.

[37] Siddharth Suman, Mohd. Kaleem Khan, and Manabendra Pathak, "Performance enhancement of solar collectors—A review," *Renewable and Sustainable Energy Reviews,* vol. 49, pp. 192-210, 2015.

[38] Francis Agyenim, Neil Hewitt, Philip Eames, and Mervyn Smyth, "A review of materials, heat transfer and phase change problem formulation for latent heat thermal energy storage systems (LHTESS)," *Renewable and Sustainable Energy Reviews,* vol. 14, pp. 615-28, 2010.

[39] Fluent 6.2 User's Guide, *Fluent Inc.,* 2006.

[40] Voller VR and Prakash C, "A fixed grid numerical modelling methodology for convection-diffusion mushy region phase-change problems," *Int J Heat and Mass Transfer,* vol. 30, pp. 1709-19, 1987.

[41] Jianfeng Yu, Ting Zhang, and Jianming Qian, "Measurement errors and uncertainties," *Electrical Motor Products. International Energy-Efficiency Standards and Testing Methods,* pp. 81-93, 2011.

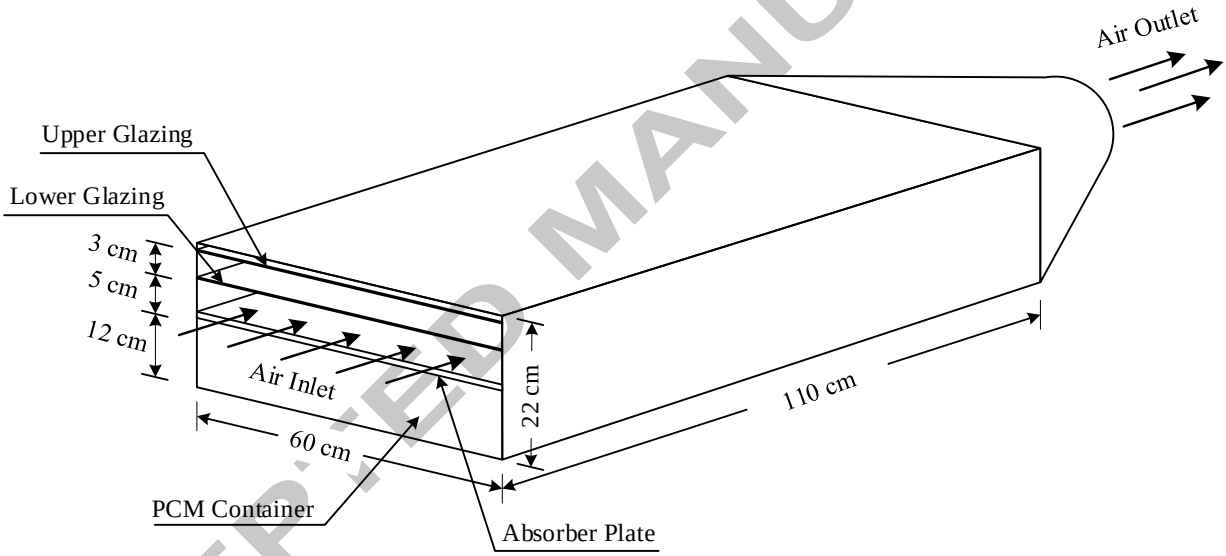

Figure 1. Schematic view of the SAH

Figure 2. Boundary conditions of the model

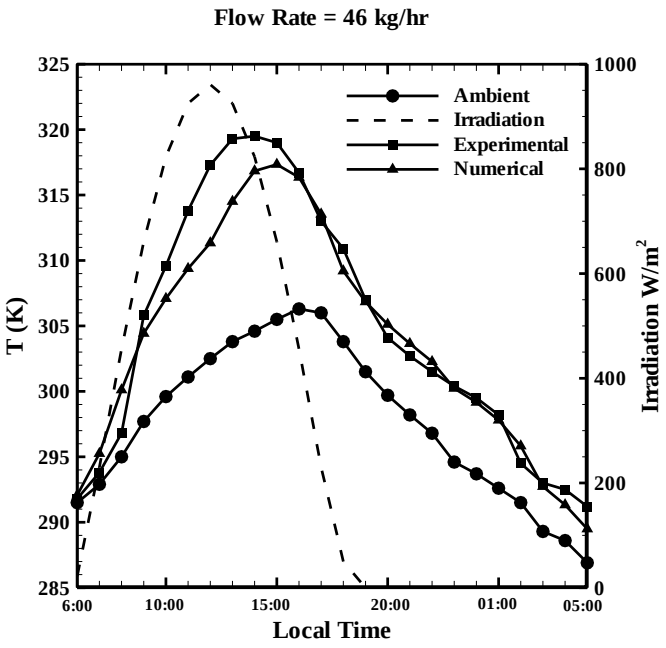

a) Temperature profiles (left axis) and solar irradiation (right axis)

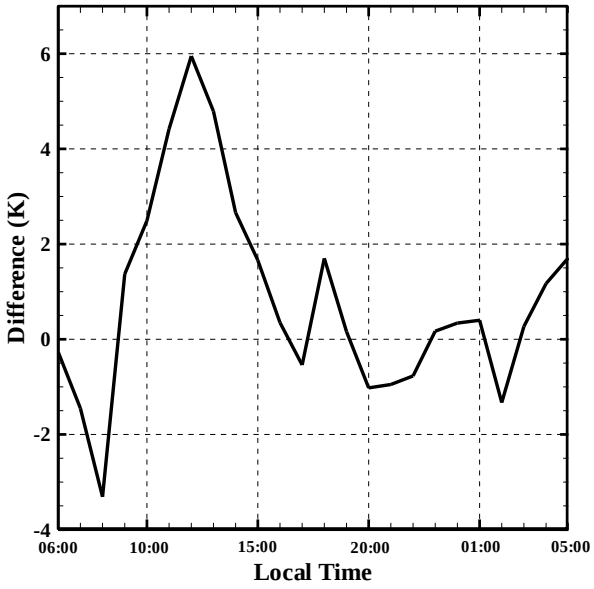

b) Difference between measured and simulated outlet temperatures

Figure 3. Comparison between numerical and experimental results on July 5

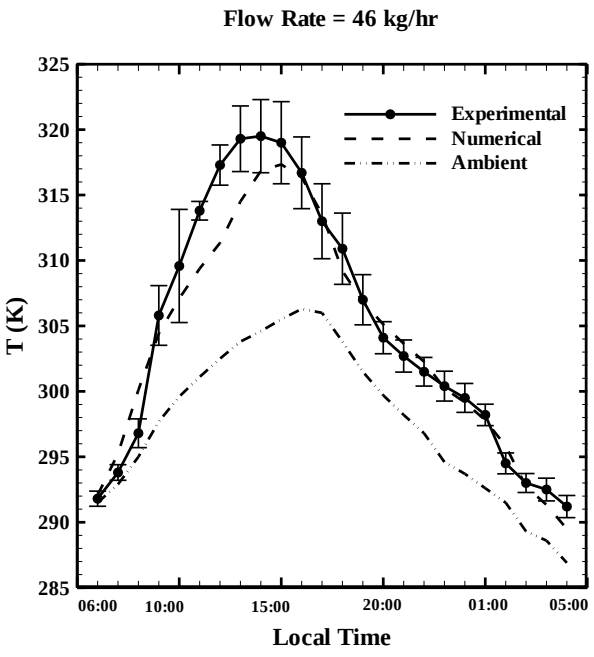

Figure 4. The hourly uncertainty of the measured outlet temperature

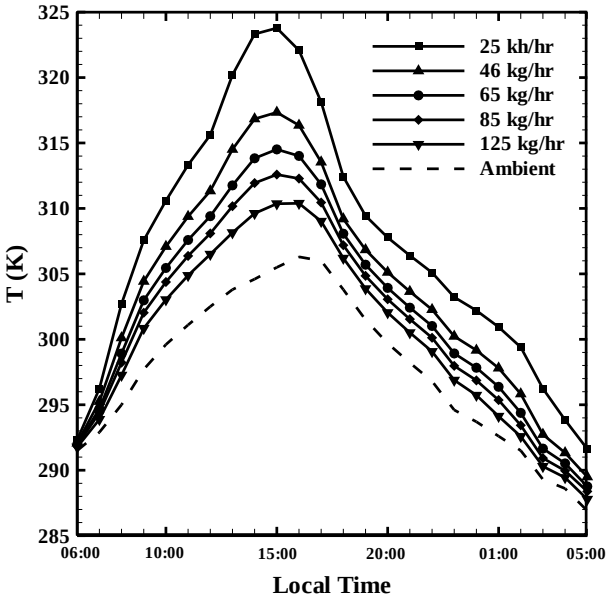

Figure 5. The outlet temperature by the air mass flow rate

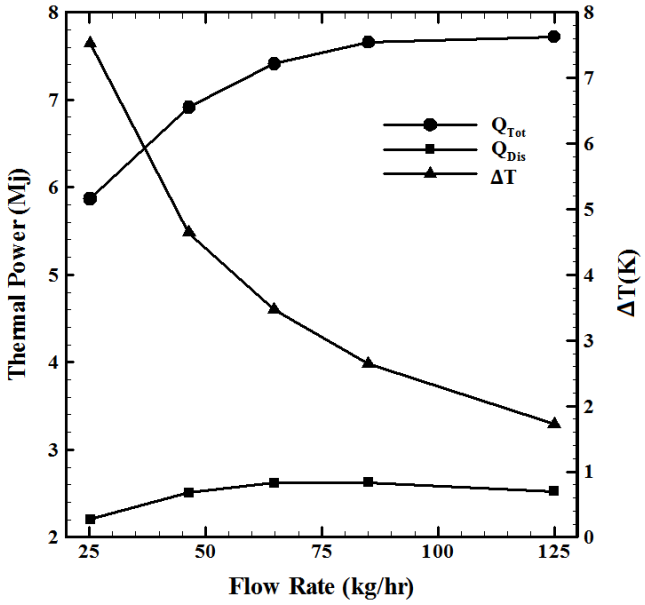

Figure 6. Thermal power (left axis) and average nocturnal temperature difference (right axis) by the air flow rate

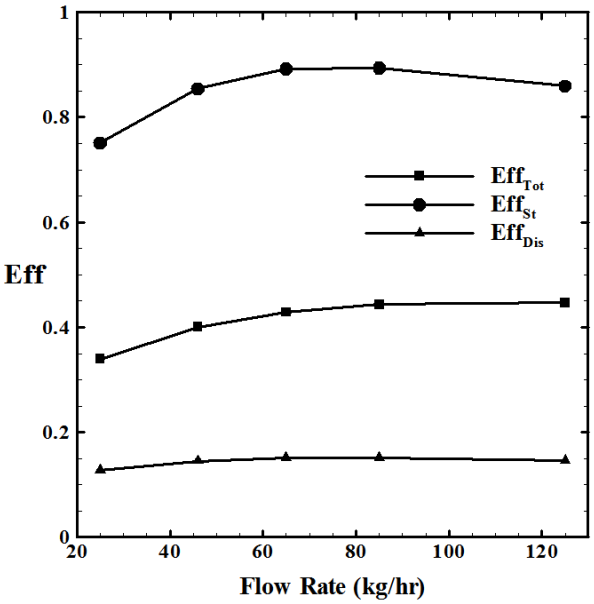

Figure 7. Total energy efficiency, discharging efficiency and energy storage efficiency by the air flow rate

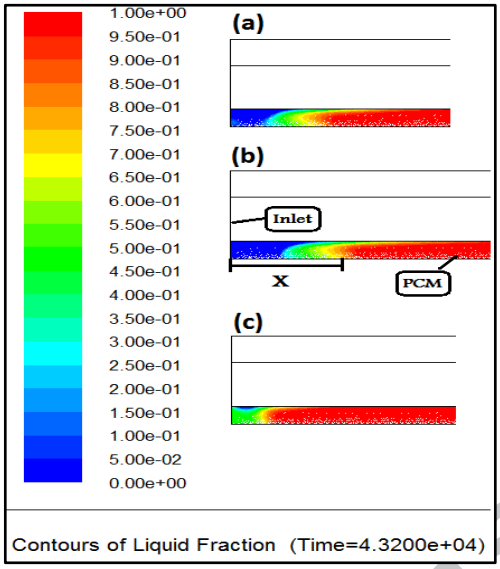

Figure 8. Phase change contours at three airflow rates: a) 85 kg/hr. b) 125 kg/hr. c) 25 kg/hr

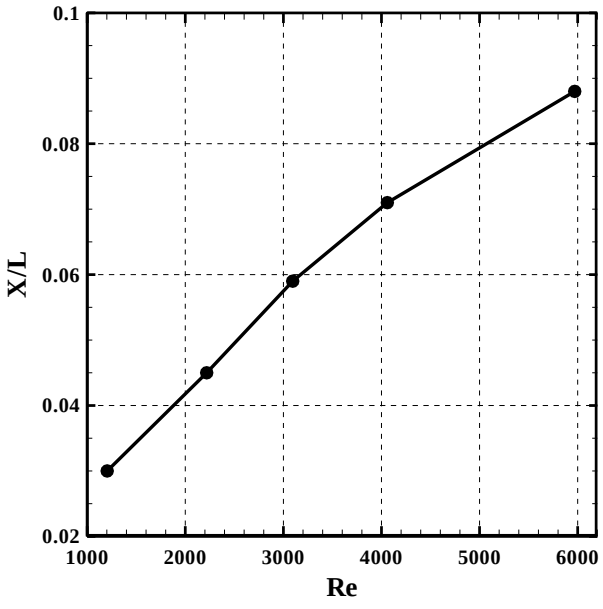

Figure 9. Dimensionless dead length by Reynolds number

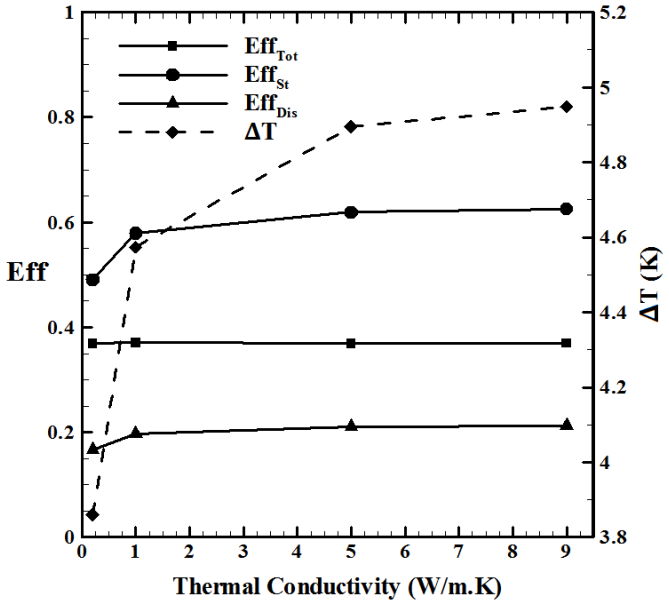

Figure 10. Total energy efficiency, discharging efficiency and energy storage efficiency (left axis) and average nocturnal temperature difference (right axis) by the thermal conductivity of paraffin

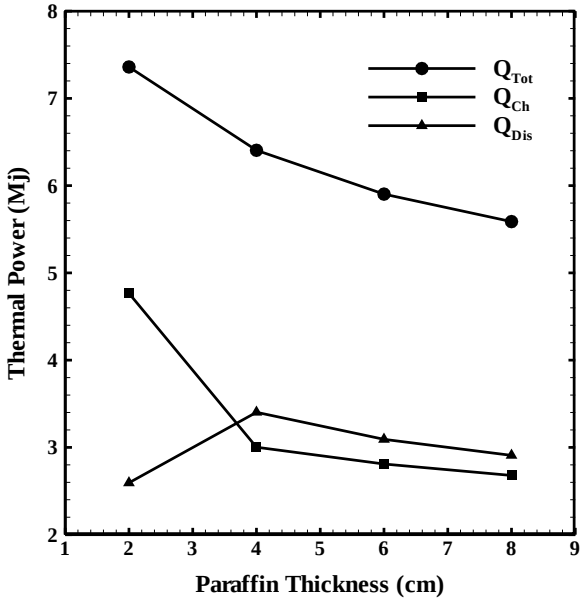

Figure 11. Total thermal power, discharging thermal power, and charging thermal power by the paraffin thickness

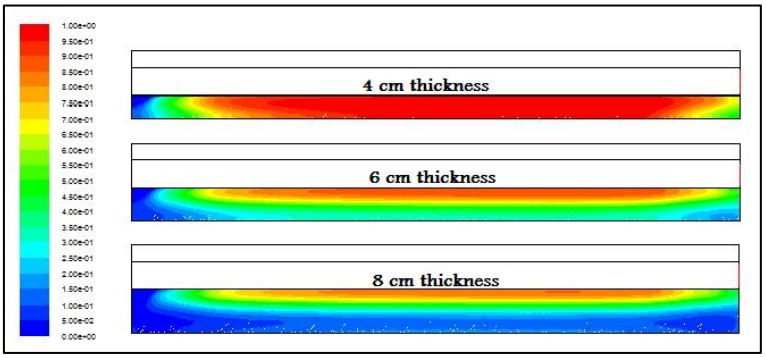

Figure 12. Contours of liquid fraction with different thickness of PCM

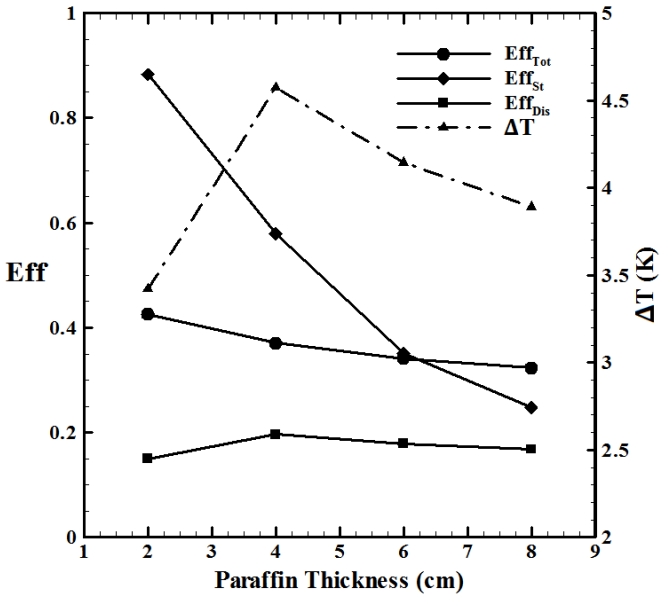

Figure 13. Total energy efficiency, discharging efficiency and energy storage efficiency (left axis) and average nocturnal temperature difference (right axis) by the paraffin thickness

Table 1. Thermal properties of the paraffin

Heat of Fusion (kJ/kg)	Thermal Conductivity (W/m.K)	Cp (J/kg.K)
250	0.2	2500
Density - solid (kg/m^3)	Density – liquid (kg/m^3)	Melting Temperature (K)
890	850	325 - 329

Table 2. Thermal properties of materials of the SAH

Material	Cp (J/kg.K)	Thermal Conductivity (W/m.K)	Density (kg/m^3)	Refractive Index
Glass	840	0.94	2600	1.526
Steel	502.48	16.27	8030	N.A.

Table 3. Standard uncertainty of outlet temperature on July 5, 2016

Local Time	$T_{out, avg}$ (K)	u_i (K)	u_{tot} (K)
6:00	293.8	0.033333	0.578312
7:00	295.8	0.145297	0.595352
8:00	298.9	0.933333	1.097472
9:00	306.9	2.206808	2.281082
10:00	314.9	4.285376	4.324093
11:00	323.3	0.416333	0.711805
12:00	327.3	1.424001	1.536591
13:00	330.2	2.441994	2.509316
14:00	331	2.733943	2.79424
15:00	328	3.083468	3.137055
16:00	325	2.681003	2.742464
17:00	319.8	2.804164	2.862982
18:00	313.8	2.662705	2.724579
19:00	307.8	1.827871	1.916884
20:00	303.8	1.078579	1.223383
21:00	302.1	1.081665	1.226105
22:00	300.8	0.927961	1.092906
23:00	299.5	0.983757	1.140663
24:00	298.4	0.940449	1.10353
1:00	297.3	0.581187	0.819214
2:00	296.4	0.550757	0.797914
3:00	295.1	0.437163	0.724185
4:00	294.3	0.648931	0.868588
5:00	293.3	0.617342	0.845248

Table 4. Summary of the results of the optimization

Flow Rate (kg/hr)	25	46	65	85	125
Eff_{tot}	0.34	0.4	0.43	0.44	0.45
ΔT (K)	7.53	4.64	3.46	2.64	1.72
Thermal Conductivity of paraffin (W/m.K)	0.2	1	5	9	N.A.
Eff_{tot}	0.37	0.37	0.37	0.37	N.A.
ΔT (K)	3.86	4.57	4.9	4.95	N.A.
Thickness of Paraffin (cm)	2	4	6	8	N.A.
Eff_{tot}	0.42	0.37	0.34	0.32	N.A.
ΔT (K)	3.42	4.6	4.15	3.89	N.A.

Highlights

- A solar air heater with phase change material is investigated.
- Effects of different parameters on the performance of the solar air heater are studied.
- The solar air heater kept the average nocturnal temperature difference of 4.5^{o}C at the best performance.
- The total energy efficiency was about 37%.
- The results of the simulation showed a good agreement with experimental.